International Journal of Innovative
Computing, Information and Control
Volume **15**, Number **5**, October **2019**

ICIC International ©2019 ISSN 1349-4198
pp. **1835–1849**

SPEED PREDICTIVE CONTROL OF FIVE-PHASE PERMANENT MAGNET SYNCHRONOUS MOTOR WITH SINGLE-PHASE OPEN FAULT

Yanwei Huang, Shaojian Tang, Wenchao Huang and Shaobin Chen

College of Electrical Engineering and Automation
Fuzhou University
No. 2, Xueyuan Road, Daxue New District, Fuzhou 350108, P. R. China
{ sjtu_huanghao; ehwenc }@fzu.edu.cn

Received January 2019; revised May 2019

Abstract. *When a single-phase open fault occurs in five-phase permanent magnet synchronous motor, there is a coupling term between the speed loop and the current loop. It is difficult to suppress the coupling term by using the predictive current control strategy with the conventional cascade structure, which results in speed and torque fluctuations and a reduction of anti-interference ability. Here, an integrated speed predictive control strategy combining speed loop with current loop is proposed to suppress the coupling term. When the motor is in fault of single-phase open, the mathematical model is derived by the coordinate transformation matrix in the α-β coordinate. It is discretized into the speed predictive model by Taylor series. The fault-tolerant current is calculated by the constraint condition of the minimum stator copper loss. Moreover, the cost function is designed with the speed and current error term, and the optimal voltage vector is determined to switch the inverter by the minimum of the cost function among the all basic voltage vectors. The simulation results show that the proposed control strategy can reduce the errors in the speed and torque for the motor system and improve an anti-interference ability by comparing with the conventional strategy.*

Keywords: Five-phase permanent magnet synchronous motor, Phase open fault, Coupling term, Fault-tolerant current, Speed predictive control

1. **Introduction.** Multi-phase permanent magnet synchronous motor (PMSM) has the characteristics of low voltage, high power, low torque ripple and strong fault tolerance [1]. It has been widely used in military equipment, aerospace [2], and ship propulsion [3]. Due to the redundancy of the number of phases, when a phase open fault occurs in the stator coil or the inverter, an appropriate fault-tolerant strategy is adopted to achieve smooth operation. It is one of the most prominent advantages from multi-phase PMSM to three-phase PMSM [4-6].

The control strategy of multi-phase PMSM is similar to that of three-phase PMSM, mainly including field-orientated control (FOC) [7], direct torque control (DTC) [8] and finite control set-model predictive control (FCS-MPC) [9]. FCS-MPC selects the optimal voltage from all basic voltage vectors according to the minimal cost function [10,11]. Compared to FOC and DTC, FCS-MPC has the advantages of simple structure, high control flexibility and better dynamic control performance [12]. For an asymmetrical six-phase PMSM with single-phase open fault, the perturbation term in α-β axis and x-y axis is derived to compensate the predictive variables to obtain accurate current predictive values to reduce the torque ripple. However, the motor model in fault is not analyzed [13]. For asymmetric double-three-phase induction motors, the predictive current control

DOI: 10.24507/ijicic.15.05.1835

(PCC) algorithm is used to regulate the current inner loop by the α-β axis current selected as the control target to reduce the stator current ripple and improve dynamic behavior [14]. A mathematical model of five-phase induction motor in the α-β coordinate is analyzed [15], and adopts the proposed control strategy in the work of [14] to realize the smooth operation of the five-phase induction motor in single-phase open fault. However, the PI controller for speed loop neglects the speed coupling term in the α-β axis current model, which results in a large fluctuation of speed and torque [15,16]. A speed predictive control (SPC) strategy is adopted to simultaneously manipulate speed and current variables by adding the error terms of speed and d-axis current into the cost function [17]. SPC selects the optimal voltage vector from all basic voltage vectors according to the minimal cost function. SPC obtains a better precision and dynamic performance by comparing with the cascade structure. However, SPC still has not been used to control multi-phase PMSM with the phase open fault.

An integrated SPC strategy is proposed for the five-phase PMSM (FPMSM) with phase open fault by combining the speed loop with the current loop. Firstly, the mathematical model with the single-phase open fault in the α-β coordinate is established by the coordinate transformation matrix. It is discretized by the Taylor series to obtain the predictive values of speed and α-β axis current. The fault-tolerant current is calculated by the constraint condition of the minimum stator copper loss and is further transformed into the expected value of the zero-sequence current. Moreover, the predictive values of d-q axis current are transformed from α-β axis. The optimal voltage vector is selected from all basic voltage vectors according to the minimal cost function with the speed and d-axis current error term. The optimal voltage vector is used to regulate the inverter. Finally, the simulation results show that SPC system can keep the motor running smoothly in the phase open fault. The speed and torque fluctuations are reduced to 1/50 and 1/3 respectively compared with the cascaded PCC system.

In this work, the mathematical model of FPMSM is derived in α-β axis in Section 2. The expected fault-tolerant current in single-phase open fault is calculated in Section 3. SPC strategy is proposed to regulate the speed and current loops in Section 4. The simulation results are provided by comparing the performance of system for the SPC strategy and cascaded PCC strategy in Section 5. The conclusions are summarized in Section 6.

2. FPMSM Model of Single-Phase Fault.

2.1. Model of single-phase open fault. For the surface-mounted FPMSM, the coils are sinusoidally distributed with star-shaped connection. When a phase open fault occurs in any coil or inverter of FPMSM (the phase short circuit fault can be converted into the phase open fault), the mathematical model of phase open can be derived from the three-phase PMSM model. Figure 1 shows the structure of FPMSM system with the assumption that the A-phase coil or the inverter is open fault in the motor system. i_a, i_b, i_c, i_d and i_e are five-phase stator currents, u_a, u_b, u_c, u_d and u_e are five-phase stator voltages, and S_a, S_b, S_c, S_d and S_e are the switching state of five-phase inverter, respectively. $S_j = 0$ or 1, where $j = a$, b, c, d, e, 0 means turn-off, and 1 means turn-on. U_{dc} is DC-link voltage. The analysis of another phase fault is similar.

The stator voltage equation and the motion equation are

$$\begin{cases} \boldsymbol{u}_s = \boldsymbol{R}\boldsymbol{i}_s + \boldsymbol{L}_s \frac{\mathrm{d}}{\mathrm{d}t}\boldsymbol{i}_s + \frac{\mathrm{d}}{\mathrm{d}t}\psi_f \\ J\frac{\mathrm{d}\omega_m}{\mathrm{d}t} = T_e - T_L - B\omega_m \\ T_e = p \cdot \boldsymbol{i}_s^{\mathrm{T}} \frac{\partial \psi_f}{\partial \theta} \end{cases} \tag{1}$$

where $\boldsymbol{u}_s = [\ u_b\ \ u_c\ \ u_d\ \ u_e\ ]^{\mathrm{T}}$ is the stator voltage vector; $\boldsymbol{i}_s = [\ i_b\ \ i_c\ \ i_d\ \ i_e\ ]^{\mathrm{T}}$ is the stator current vector; $\boldsymbol{R} = \mathrm{diag}[\ R\ \ R\ \ R\ \ R\ ]$, R is the stator resistance; $\boldsymbol{L}_s$ is the stator inductance matrix; ψ_f is the permanent magnet flux linkage to the axis of the remaining phase windings; ω_m is the mechanical angular velocity of the motor; T_e is the electromagnetic torque; T_L is the load torque; J is the motor inertia; B is the friction coefficient; p is the pole pairs.

$$\boldsymbol{L}_s = L_l \begin{bmatrix} 1 & 0 & 0 & 0 \\ 0 & 1 & 0 & 0 \\ 0 & 0 & 1 & 0 \\ 0 & 0 & 0 & 1 \end{bmatrix} + L_m \begin{bmatrix} 1 & \cos\delta & \cos 2\delta & \cos 3\delta \\ \cos\delta & 1 & \cos\delta & \cos 2\delta \\ \cos 2\delta & \cos\delta & 1 & \cos\delta \\ \cos 3\delta & \cos 2\delta & \cos\delta & 1 \end{bmatrix} \tag{2}$$

$$\boldsymbol{\psi}_f = \psi_f \begin{bmatrix} \cos(\theta - \delta) \\ \cos(\theta - 2\delta) \\ \cos(\theta - 3\delta) \\ \cos(\theta - 4\delta) \end{bmatrix} \tag{3}$$

In Equation (2) and Equation (3), δ is the angle of the stator coil spatial position, $\delta = 2/5\pi$; L_l is the stator leakage inductance; L_m is the inductance amplitude; ψ_f is the permanent magnet flux amplitude; θ is the electrical angle of motor rotor.

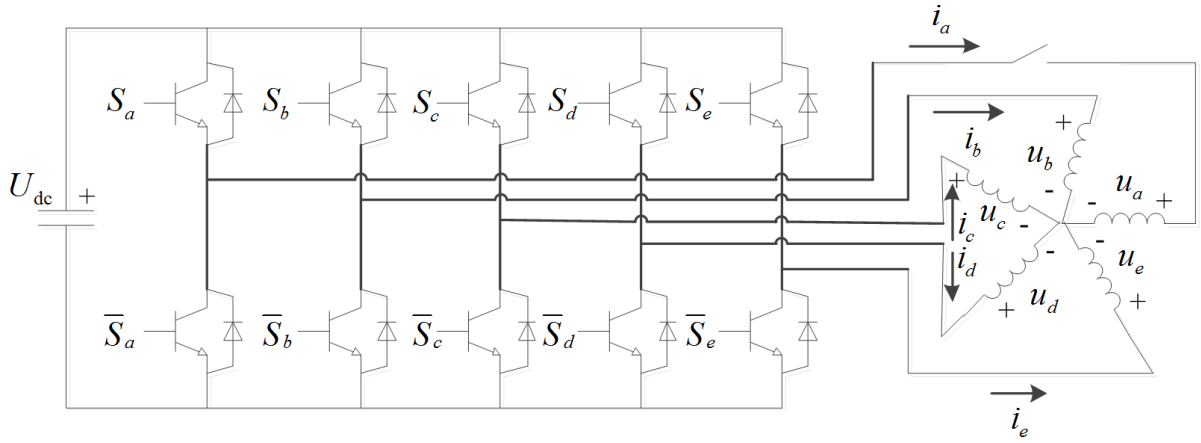

FIGURE 1. FPMSM system

2.2. **Clark transform matrix with single-phase open fault.** From Equation (1) and Equation (2), the phase voltage has relationship between the self-phase current, and other phase currents and rotor position. It has too many coupling terms and is difficult to analyze and control. In order to obtain a decoupling mathematical model by eliminating the coupling terms, Equation (1) is transformed into the α-β model by Clark transformation matrix.

In α-β axis, the center of A, B, C, D, E five-phase coil is the axis origin O, the axis of the A-phase is selected as the α-axis, and the angle between the β-axis and the α-axis is 90°, in Figure 2.

For A-phase open fault, the Clark transform matrix $\boldsymbol{T}_{\alpha\beta}$ is

$$\boldsymbol{T}_{\alpha\beta} = [\ \boldsymbol{\alpha}\ \ \boldsymbol{\beta}\ \ \boldsymbol{x}\ \ \boldsymbol{y}\ ]^{\mathrm{T}} \tag{4}$$

where $\boldsymbol{x}$ and $\boldsymbol{y}$ vectors are zero-sequence components to make $\boldsymbol{T}_{\alpha\beta}$ become an orthogonal matrix. To map B, C, D, and E axis into α-axis and β-axis, $\boldsymbol{\alpha}$ and $\boldsymbol{\beta}$ vectors are defined

as

$$\begin{aligned} \boldsymbol{\alpha} &= \left[\begin{array}{cccc} \cos\delta & \cos 2\delta & \cos 3\delta & \cos 4\delta \end{array} \right] \\ \boldsymbol{\beta} &= \left[\begin{array}{cccc} \sin\delta & \sin 2\delta & \sin 3\delta & \sin 4\delta \end{array} \right] \end{aligned} \tag{5}$$

When the motor is in a healthy state, $\boldsymbol{\alpha} = [\cos 0 \ \ \cos\delta \ \ \cos 2\delta \ \ \cos 3\delta \ \ \cos 4\delta]$, and $\boldsymbol{\beta} = [\sin 0 \ \ \sin\delta \ \ \sin 2\delta \ \ \sin 3\delta \ \ \sin 4\delta]$. They satisfy $\cos 0 + \cos\delta + \cos 2\delta + \cos 3\delta + \cos 4\delta = 0$ and $\sin 0 + \sin\delta + \sin 2\delta + \sin 3\delta + \sin 4\delta = 0$, respectively. The sum of the phase currents should be zero due to the coils with star-shaped connection, i.e., $i_a + i_b + i_c + i_d + i_e = 0$. Moreover, the vector $\boldsymbol{y}$ is selected as $\boldsymbol{y} = [1/2 \ \ 1/2 \ \ 1/2 \ \ 1/2 \ \ 1/2]$, and satisfies $\boldsymbol{\beta}\boldsymbol{y}^{\mathrm{T}} = 0$, which is orthogonal to the vector $\boldsymbol{\beta}$.

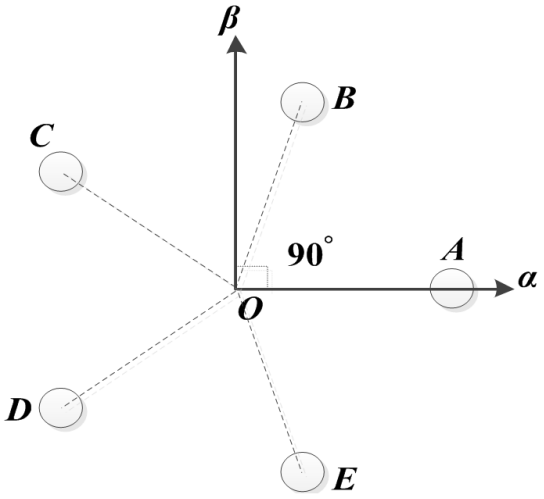

FIGURE 2. Relationship between α-β axis and five-phase axis

In the single-phase open fault, the vector $\boldsymbol{y}$ is taken as

$$\boldsymbol{y} = \left[\begin{array}{cccc} \frac{1}{2} & \frac{1}{2} & \frac{1}{2} & \frac{1}{2} \end{array} \right] \tag{6}$$

Equation (5) and Equation (6) show that $\boldsymbol{\alpha}\boldsymbol{y}^{\mathrm{T}} = 1/2(\cos\delta + \cos 2\delta + \cos 3\delta + \cos 4\delta) = -1/2$, the vector $\boldsymbol{y}$ is not orthogonal to vector $\boldsymbol{\alpha}$. In order to satisfy the orthogonal relationship between vector $\boldsymbol{\alpha}$ and vector $\boldsymbol{y}$, the vector $\boldsymbol{\alpha}$ is changed to $\boldsymbol{\alpha}_1$,

$$\boldsymbol{\alpha}_1 = \left[\begin{array}{cccc} \frac{1}{4} + \cos\delta & \frac{1}{4} + \cos 2\delta & \frac{1}{4} + \cos 3\delta & \frac{1}{4} + \cos 4\delta \end{array} \right] \tag{7}$$

From Equation (7) and Equation (6), vector $\boldsymbol{\alpha}_1$ and vector $\boldsymbol{y}$ satisfy the orthogonal relationship with $\boldsymbol{\alpha}_1\boldsymbol{y}^{\mathrm{T}} = 0$. From Equation (7) and Equation (5), vector $\boldsymbol{\alpha}_1$ and vector $\boldsymbol{\beta}$ also satisfy the orthogonal relationship with $\boldsymbol{\alpha}_1\boldsymbol{\beta}^{\mathrm{T}} = 0$. In single-phase open fault, under the condition that the sum of phase current and voltage is zero, i.e., $i_b + i_c + i_d + i_e = 0$ and $u_b + u_c + u_d + u_e = 0$, the vector $\boldsymbol{\alpha}_1$ satisfies the Clark transformation condition.

When the vectors $\boldsymbol{\alpha}_1$, $\boldsymbol{\beta}$, and $\boldsymbol{y}$ are determined, the vector $\boldsymbol{x}$ can be obtained by satisfying the equation $\boldsymbol{x}\boldsymbol{\alpha}_1^{\mathrm{T}} = 0$, $\boldsymbol{x}\boldsymbol{\beta}^{\mathrm{T}} = 0$ and $\boldsymbol{x}\boldsymbol{y}^{\mathrm{T}} = 0$,

$$\boldsymbol{x} = \left[\begin{array}{cccc} -\sin 2\delta & \sin\delta & \sin 4\delta & -\sin 3\delta \end{array} \right] \tag{8}$$

In single-phase open fault, the Clark transformation matrix $\boldsymbol{T}_{\alpha\beta}$ is redesigned as

$$\boldsymbol{T}_{\alpha\beta} = \lambda \begin{bmatrix} \frac{1}{4}+\cos\delta & \frac{1}{4}+\cos 2\delta & \frac{1}{4}+\cos 3\delta & \frac{1}{4}+\cos 4\delta \\ \sin\delta & \sin 2\delta & \sin 3\delta & \sin 4\delta \\ -\sin 2\delta & \sin\delta & \sin 4\delta & -\sin 3\delta \\ \frac{1}{2} & \frac{1}{2} & \frac{1}{2} & \frac{1}{2} \end{bmatrix} \tag{9}$$

In Equation (9), λ is a coefficient to guarantee that the amplitudes are consistent before and after the Clark transformation, where $\lambda = 2/5$.

2.3. ***α-β* axis mathematical model with single-phase open fault.** The Clark transformation matrix $\boldsymbol{T}_{\alpha\beta}$ with Equation (9) is left-multiplied to the stator voltage $\boldsymbol{u}_s$ Equation (1),

$$\boldsymbol{T}_{\alpha\beta}\boldsymbol{u}_s = \boldsymbol{T}_{\alpha\beta}\boldsymbol{R}\boldsymbol{T}_{\alpha\beta}^{-1}\cdot\boldsymbol{T}_{\alpha\beta}\boldsymbol{i}_s + \boldsymbol{T}_{\alpha\beta}\boldsymbol{L}_s\boldsymbol{T}_{\alpha\beta}^{-1}\cdot\frac{\mathrm{d}}{\mathrm{d}t}(\boldsymbol{T}_{\alpha\beta}\boldsymbol{i}_s) + \boldsymbol{T}_{\alpha\beta}\cdot\frac{\mathrm{d}}{\mathrm{d}t}\psi_f \tag{10}$$

Equation (10) is the mathematical model of FPMSM with single-phase open fault in the α-β axis. Since the sum of the phase currents satisfies $(i_b + i_c + i_d + i_e)/2 = 0$, the fourth row in the zero-sequence variable can be neglected in Equation (10)

$$\boldsymbol{u}_{\alpha\beta} = \boldsymbol{R}\boldsymbol{i}_{\alpha\beta} + \boldsymbol{L}_{\alpha\beta}\cdot\frac{\mathrm{d}}{\mathrm{d}t}\boldsymbol{i}_{\alpha\beta} + \psi \tag{11}$$

where $\boldsymbol{u}_{\alpha\beta} = \boldsymbol{T}_{\alpha\beta}\cdot\boldsymbol{u}_s = [u_\alpha\ \ u_\beta\ \ u_z]^{\mathrm{T}}$, u_α, u_β and u_z are α-β axis stator voltage and zero-sequence voltage, respectively; $\boldsymbol{i}_{\alpha\beta} = \boldsymbol{T}_{\alpha\beta}\cdot\boldsymbol{i}_s = [i_\alpha\ \ i_\beta\ \ i_z]^{\mathrm{T}}$, i_α, i_β and i_z are α-β axis stator current and zero-sequence current, respectively; $\boldsymbol{L}_{\alpha\beta} = \boldsymbol{T}_{\alpha\beta}\cdot\boldsymbol{L}_s\cdot\boldsymbol{T}_{\alpha\beta}^{-1} = \mathrm{diag}[L_\alpha, L_\beta, L_l]$, L_α and L_β are α-β axis equivalent stator inductances, respectively, and $L_\alpha = 1.25L_m + L_l$, $L_\beta = 2.5L_m + L_l$; $\boldsymbol{\psi} = \mathrm{d}(\boldsymbol{T}_{\alpha\beta}\cdot\boldsymbol{\psi}_f)/\mathrm{d}t = \omega\psi_f[-0.5\sin\theta\ \ \cos\theta]^{\mathrm{T}}$, ω is the electrical angular velocity, $\omega = p\cdot\omega_m$.

The electromagnetic torque in Equation (1) is also transformed as

$$T_e = p\cdot\left(\boldsymbol{T}_{\alpha\beta}^{-1}\boldsymbol{i}_{\alpha\beta}\right)^{\mathrm{T}}\frac{\partial\boldsymbol{\psi}_f}{\partial\theta} = \frac{5}{2}p\psi_f(i_\beta\cos\theta - i_\alpha\sin\theta) \tag{12}$$

From Equation (11), Equation (12) and Equation (1), the mathematical model of F-PMSM with single-phase open fault in α-β axis is obtained,

$$\begin{cases} \dfrac{di_\alpha}{dt} = \dfrac{1}{L_\alpha}u_\alpha - \dfrac{R}{L_\alpha}i_\alpha + \dfrac{\omega\psi_f\sin\theta}{2L_\alpha} & \text{(a)} \\ \dfrac{di_\beta}{dt} = \dfrac{1}{L_\beta}u_\beta - \dfrac{R}{L_\beta}i_\beta - \dfrac{\omega\psi_f\cos\theta}{2L_\beta} & \text{(b)} \\ \dfrac{di_z}{dt} = \dfrac{1}{L_l}u_z - \dfrac{R}{L_l}i_z & \text{(c)} \\ \dfrac{d\omega}{dt} = -\dfrac{B}{J}\omega + \dfrac{p}{J}T_e - \dfrac{p}{J}T_L & \text{(d)} \\ T_e = \dfrac{5}{2}p\psi_f(i_\beta\cos\theta - i_\alpha\sin\theta) & \text{(e)} \end{cases} \tag{13}$$

In Equation (13), (a), (b) and (c) are the current loops of the FPMSM, and the α-β axis current loops are affected by the speed coupling term: $\omega\psi_f\sin\theta/(2L_\alpha)$ and $\omega\psi_f\cos\theta/(2L_\beta)$, and the electromagnetic torque T_e of the speed loop is directly affected by i_α and i_β. If the cascaded PCC strategy is used by proposed in [15], a current loop predictive controller is designed for Equation (13)(a), (13)(b) and (13)(c), and a PI speed controller is designed for Equation (13)(d). The PCC strategy is a very practical control

scheme. However, due to the coupling terms between the inner and outer loops, the PCC strategy is a cascade structure and is difficult to suppress the coupling terms between the current loop and the speed loop PCC is difficult to improve the control accuracy and anti-interference ability.

In order to improve the anti-interference ability for suppressing coupling terms, the predictive control method is used to directly regulate the speed. The cost function is designed by adding the speed and current variables, and an SPC method combining speed loop with current loop in single-phase open fault is proposed to suppress the coupling terms for a better system performance.

3. **Fault-Tolerant Current in Single-Phase Open Fault.** For single-phase open fault in FPMSM, the electromagnetic field generated by the coils of remaining four phases will be distorted to worsen the speed performance, and to increase the copper loss of the coils. To reproduce a continuous spatial electromagnetic field in single-phase open fault, the expected fault-tolerant currents of the remaining four phases are re-solved to make FPMSM operate normally.

The magnetomotive force at the angle γ related to the axis of A-phase is

$$\begin{aligned} F_A &= F_b + F_c + F_d + F_e \\ &= 0.5Ni_b\cos(\gamma-\delta) + 0.5Ni_c\cos(\gamma-2\delta) + 0.5Ni_d\cos(\gamma-3\delta) \\ &\quad + 0.5Ni_e\cos(\gamma-4\delta) \end{aligned} \tag{14}$$

where N is the number of the coil.

When FPMSM is in a healthy state, the magnetomotive force at the angle γ related to the axis of A-phase is

$$F = 1.25NI_m\sin(\omega t-\gamma) \tag{15}$$

where I_m is the amplitude of current.

In order to run smoothly in phase open fault, Equation (14) and Equation (15) are equal according to the principle that remains the magnetomotive force consistent before and after phase open fault,

$$F_A = F \tag{16}$$

In phase open fault, B, C, D, and E phase currents are

$$\begin{cases} i_b = x_bI_m\sin\omega t + y_bI_m\cos\omega t \\ i_c = x_cI_m\sin\omega t + y_cI_m\cos\omega t \\ i_d = x_dI_m\sin\omega t + y_dI_m\cos\omega t \\ i_e = x_eI_m\sin\omega t + y_eI_m\cos\omega t \end{cases} \tag{17}$$

where the coefficients x_i and y_i, $i = b, c, d, e$ are to be solved.

Substituting Equation (17) into Equation (16),

$$\begin{cases} 0.309x_b - 0.809x_c - 0.809x_d + 0.309x_e = 2.5 \\ 0.309y_b - 0.809y_c - 0.809y_d + 0.309y_e = 0 \\ 0.9511y_b + 0.5878y_c - 0.5878y_d - 0.9511y_e = -2.5 \\ 0.9511x_b + 0.5878x_c - 0.5878x_d - 0.9511x_e = 0 \end{cases} \tag{18}$$

Since the coils of FPMSM are the star-shaped connection, x_i and y_i also satisfy the condition

$$\begin{cases} x_b + x_c + x_d + x_e = 0 \\ y_b + y_c + y_d + y_e = 0 \end{cases} \tag{19}$$

From Equation (18) and Equation (19), six equations contain eight unknown variables, which result in the infinite solutions on x_i and y_i. They can be solved unique by adding constraints from actual control requirements. In this work, the expected fault-tolerant

current is solved with the constraint condition of the minimal stator copper loss. The expression of the stator copper loss for single-phase open fault in FPMSM is

$$P_{cu} = I_b^2 R + I_c^2 R + I_d^2 R + I_e^2 R \tag{20}$$

where I_i is the effective value of the i-phase current, $i = b, c, d, e$, and $I_i = I_m\sqrt{(x_i^2 + y_i^2)/2}$. Equation (20) is the objective function with Equation (18) and Equation (19) as the constraints. In order to obtain the minimum value of the stator copper loss P_{cu} in Equation (20), λ_n is introduced to construct Lagrange function [18], where $n = 1 \sim 6$. The partial derivative of Lagrange function to x_i, y_i and λ_n are equal to zero to get 14 equations, the unique solutions by solving the 14 equations is: $\lambda_1 = 2R$, $\lambda_2 = 0$, $\lambda_3 = -R$, $\lambda_4 = 0$, $\lambda_5 = 0.5R$, $\lambda_6 = 0$, and the unique solutions of x_i and y_i are

$$\begin{cases} x_b = 1.118 \\ x_c = -1.118 \\ x_d = -1.118 \\ x_e = 1.118 \end{cases} \quad \begin{cases} y_b = 0.951 \\ y_c = 0.588 \\ y_d = -0.588 \\ y_e = -0.951 \end{cases} \tag{21}$$

The expressions of expected fault-tolerant currents i_b^*, i_c^*, i_d^* and i_e^* with the minimal stator copper loss are obtained from Equation (17)

$$\begin{cases} i_b^* = 1.468 I_m \cos(\omega t - 49.6^\circ) \\ i_c^* = 1.263 I_m \cos(\omega t + 62.3^\circ) \\ i_d^* = 1.263 I_m \cos(\omega t + 117.7^\circ) \\ i_e^* = 1.468 I_m \cos(\omega t + 229.6^\circ) \end{cases} \tag{22}$$

Equation (22) shows the expected B, C, D, and E phase currents in single-phase open fault of the FPMSM. At this time, the stator copper loss is minimal.

After obtaining the expected four-phase current expressions i_b^*, i_c^*, i_d^* and i_e^*, the expected current of d-q axis and α-β axis can be obtained by transforming i_b^*, i_c^*, i_d^* and i_e^* into d-q axis and α-β axis. The SPC strategy is used to make the output current track the expected current accurately and obtain the optimal performance in single-phase open fault.

4. SPC Strategy of FPMSM in Single-Phase Open Fault.

The main idea of SPC strategy is to simultaneously calculate the discretized model of the FPMSM in Equation (13)(a)-(13)(d) to obtain the predictive values corresponding to each basic voltage vector, which are substituted into the cost function with the speed and d-axis current error term. Moreover, the optimal voltage vector is selected to regulate the inverter according to the minimal cost function. Figure 3 shows the basic control structure diagram, including the cost function and the predictive model.

4.1. The discretized model by Taylor series.

In order to obtain the predictive value of the state variable, Equation (13) is discretized by the Taylor series expansion. The Taylor series expansion is described as

$$x(k+1) = x(k) + \sum_{l=1}^{\infty} \frac{T^l}{l!} \frac{d^l x}{dt^l}\bigg|_{t=k} \tag{23}$$

where $x(k) = x(kT)$ is the value of state variable at k time, l is the order number.

In Equation (13), the α-β axis current i_α and i_β have the relation of first-order differential with the input voltages u_α and u_β, and ω has the relation of second-order differential

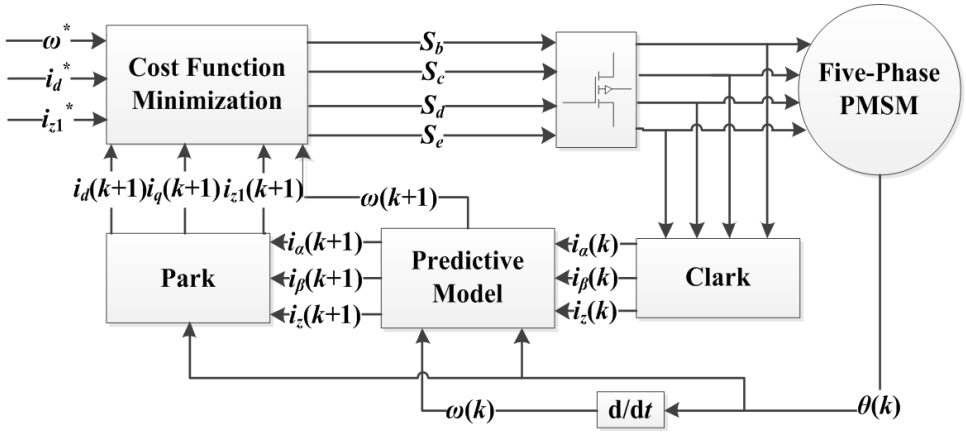

FIGURE 3. Control structure of SPC strategy

with the input voltages u_α and u_β. So first-order truncation is used for i_α and i_β, and second-order truncation is used for ω. Equation (13) is discretized as

$$i_\alpha(k+1) = \left(1 - \frac{TR}{L_\alpha}\right) i_\alpha(k) + \frac{T}{L_\alpha} u_\alpha(k) + \frac{0.5T\psi_f}{L_\alpha}\omega(k)\sin[\theta(k)] \tag{24}$$

$$i_\beta(k+1) = \left(1 - \frac{TR}{L_\beta}\right) i_\beta(k) + \frac{T}{L_\beta} u_\beta(k) - \frac{T\psi_f}{L_\beta}\omega(k)\cos[\theta(k)] \tag{25}$$

$$i_z(k+1) = \left(1 - \frac{TR}{L_l}\right) i_z(k) + \frac{T}{L_l} u_z(k) \tag{26}$$

$$\begin{aligned}
&\omega\,(k+1)\\
&= \frac{5p^2\psi_f BT^2}{4J^2}\left\{\left[\left(\frac{JR}{BL_\alpha}+1\right)\sin[\theta(k)] - \frac{J}{B}\omega(k)\cos[\theta(k)]\right] i_\alpha(k)\right.\\
&\quad \left. - \left[\left(\frac{JR}{BL_\beta}+1\right)\cos[\theta(k)] + \frac{J}{B}\omega(k)\sin[\theta(k)]\right] i_\beta(k)\right\}\\
&\quad + \left(1 - \frac{BT}{J} + \frac{B^2T^2}{2J^2} - \frac{5p^2\psi_f^2T^2}{4JL_\beta}\cos^2[\theta(k)] - \frac{5p^2\psi_f^2T^2}{8JL_\alpha}\sin^2[\theta(k)]\right)\omega(k)\\
&\quad + \frac{5p^2\psi_f T^2\cos[\theta(k)]}{4JL_\beta}u_\beta(k) - \frac{5p^2\psi_f T^2\sin[\theta(k)]}{4JL_\alpha}u_\alpha(k) + \left(\frac{BpT^2}{2J^2} - \frac{pT}{J}\right)T_L
\end{aligned} \tag{27}$$

where $i_\alpha(k+1)$, $i_\beta(k+1)$, $i_z(k+1)$, and $\omega(k+1)$ are the predictive values of state variables at $k+1$ time, respectively; $i_\alpha(k)$, $i_\beta(k)$, $i_z(k)$, and $\omega(k)$ are the values of state variables at k time; $u_\alpha(k)$, $u_\beta(k)$, and $u_z(k)$ are α-β axis voltages and zero-sequence voltage, respectively; T is the sampling period.

4.2. **The cost function.** In SPC strategy, the speed and current error terms are added into the cost function to regulate speed directly. The cost function is designed as

$$\begin{aligned}
F_c = {} & \lambda_\omega\left(\omega^*(k+1) - \omega(k+1)\right)^2 + \lambda_{id}\left(i_d^*(k+1) - i_d(k+1)\right)^2\\
& + \lambda_{iz}\left(i_{z1}^*(k+1) - i_{z1}(k+1)\right)^2 + f\left(i_{d\max}, i_{q\max}, i_{z\max}\right)
\end{aligned} \tag{28}$$

where

$$\begin{aligned}
&f(i_{d\max}, i_{q\max}, i_{z\max})\\
&= \begin{cases} \infty & |i_q(k+1)| > i_{q\max} \text{ or } |i_d(k+1)| > i_{d\max} \text{ or } |i_{z1}(k+1)| > i_{z\max}\\ 0 & |i_q(k+1)| \le i_{q\max} \text{ and } |i_d(k+1)| \le i_{d\max} \text{ and } |i_{z1}(k+1)| \le i_{z\max} \end{cases}
\end{aligned} \tag{29}$$

Equation (29) is the overcurrent protection term, where $i_{d\max}$, $i_{q\max}$, and $i_{z\max}$ are the upper limits of the d-q axis currents and the zero-sequence current, respectively. When the d-q axis currents or the zero-sequence current exceed $i_{d\max}$, $i_{q\max}$, and $i_{z\max}$, Equation (29) is set to infinity, and the corresponding basic voltage vector is not selected as the optimal voltage vector. When the d-q axis currents and the zero sequence current are lower than $i_{d\max}$, $i_{q\max}$, and $i_{z\max}$, Equation (29) is set to zero, which has no effect for selecting the optimal voltage vector.

The predictive currents of d-q axis and zero-sequence component $i_d(k+1)$, $i_q(k+1)$ and $i_{z1}(k+1)$ are obtained by Park transformation from $i_\alpha(k+1)$, $i_\beta(k+1)$, and $i_z(k+1)$

$$\begin{bmatrix} i_d(k+1) \\ i_q(k+1) \\ i_{z1}(k+1) \end{bmatrix} = \begin{bmatrix} \cos\theta & \sin\theta & 0 \\ -\sin\theta & \cos\theta & 0 \\ 0 & 0 & 1 \end{bmatrix} \begin{bmatrix} i_\alpha(k+1) \\ i_\beta(k+1) \\ i_z(k+1) \end{bmatrix} \tag{30}$$

The Park transformation matrix is

$$\boldsymbol{T}_{dq} = \begin{bmatrix} \cos\theta & \sin\theta & 0 & 0 \\ -\sin\theta & \cos\theta & 0 & 0 \\ 0 & 0 & 1 & 0 \\ 0 & 0 & 0 & 1 \end{bmatrix} \tag{31}$$

Since the fourth row in the zero-sequence variable is neglected in Equation (10), the Park transformation matrix in Equation (31) only performs the first three rows in Equation (30).

In Equation (28), $\omega^*(k+1)$, $i_d^*(k+1)$, and $i_{z1}^*(k+1)$ are the expected speed, d-axis current, and zero-sequence current, respectively. The control method with $i_d^* = 0$ is used in this work, and the i_{z1}^* can be obtained from Equation (22) by Clark transformation in Equation (9) and Park transformation in Equation (31), the result is $i_{z1}^* = 0$. Moreover, the weight coefficients λ_ω, λ_{id}, and λ_{iz} are introduced for balancing the difference dimensions.

4.3. **The selection of optimal voltage vector.** In A-phase open fault, the relationship between the phase voltage and the switching state of the inverter is

$$\begin{bmatrix} u_b \\ u_c \\ u_d \\ u_e \end{bmatrix} = \frac{1}{4}U_{dc} \begin{bmatrix} 3 & -1 & -1 & -1 \\ -1 & 3 & -1 & -1 \\ -1 & -1 & 3 & -1 \\ -1 & -1 & -1 & 3 \end{bmatrix} \begin{bmatrix} S_b \\ S_c \\ S_d \\ S_e \end{bmatrix} \tag{32}$$

$[S_b\ S_c\ S_d\ S_e] = [0\ 0\ 0\ 0] \sim [1\ 1\ 1\ 1]$ is the 16 different combinations of switching state in remaining four-phase bridge arms. The 16 groups of u_b, u_c, u_d and u_e are obtained by substituting different combinations into Equation (32). Each group of u_b, u_c, u_d and u_e synthesizes a basic voltage vector in space and each basic voltage vector determines a switching state. In Figure 4, $u_0 \sim u_{15}$ are corresponding to $[S_b\ S_c\ S_d\ S_e] = [0\ 0\ 0\ 0] \sim [1\ 1\ 1\ 1]$ respectively, where u_0 and u_{15} are zero voltage vectors, and $u_1 \sim u_{14}$ are non-zero voltage vectors. Table 1 shows the magnitude and angle of the basic voltage vectors $u_0 \sim u_{15}$ in Figure 4.

When all basic voltage vectors are defined, the zero voltage vector $u_{0(15)}$ and the non-zero voltage vectors $u_1 \sim u_{14}$ can be transformed into the corresponding α-β axis voltage u_α and u_β by Clark transformation. The predictive values $i_\alpha(k+1)$, $i_\beta(k+1)$, $i_z(k+1)$ and $\omega(k+1)$ are calculated by substituting u_α and u_β into Equations (24)-(27), the $i_d(k+1)$, $i_q(k+1)$ and $i_{z1}(k+1)$ are obtained by Park transformation to calculate 15 different values of the cost function. The optimal voltage vector is determined by the minimal cost function to switch the inverter. Moreover, the zero voltage vector is determined by the

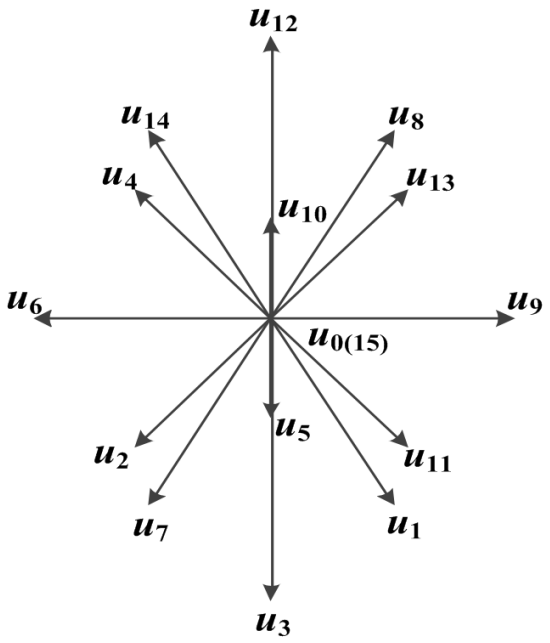

FIGURE 4. Voltage vector in A-phase open fault

TABLE 1. The magnitude (M) and angle (A) of the basic voltage vector

A \ M	**0**	$\mathbf{0.145}U_{dc}$	$\mathbf{0.325}U_{dc}$	$\mathbf{0.441}U_{dc}$	$\mathbf{0.447}U_{dc}$	$\mathbf{0.616}U_{dc}$
0°	u_0, u_{15}	×	×	×	u_9	×
46.4°	×	×	u_{13}	×	×	×
59.5°	×	×	×	u_8	×	×
90°	×	u_{10}	×	×	×	u_{12}
120.5°	×	×	×	u_{14}	×	×
133.6°	×	×	u_4	×	×	×
180°	×	×	×	×	u_6	×
226.4°	×	×	u_2	×	×	×
239.5°	×	×	×	u_7	×	×
270°	×	u_5	×	×	×	u_3
300.5°	×	×	×	u_1	×	×
313.6°	×	×	u_{11}	×	×	×

principle of minimal switching times, i.e., when the voltage vector is selected as $u_7(0111)$, $u_{11}(1011)$, $u_{13}(1101)$, $u_{14}(1110)$ at the previous time, the zero vector can be selected as $u_{15}(1111)$ at the current time; otherwise, the zero vector is selected as $u_0(0000)$.

In summary, the implemental steps of SPC strategy are

1) The state variables of system are given, $i_\alpha(k)$, $i_\beta(k)$, $i_z(k)$, $\omega(k)$, $\theta(k)$; when $k = 0$, the initial values of the state variables are: $i_\alpha(k) = 0$, $i_\beta(k) = 0$, $i_z(k) = 0$, $\omega(k) = 0$, and $\theta(k) = 0$;

2) 15 different basic voltage vectors and $i_\alpha(k)$, $i_\beta(k)$, $i_z(k)$, $\omega(k)$, $\theta(k)$ are substituted into Equation (24), Equation (25), Equation (26), and Equation (27) to obtain the corresponding predictive values $i_\alpha(k+1)$, $i_\beta(k+1)$, $i_z(k+1)$, $\omega(k+1)$. Then, $i_\alpha(k+1)$, $i_\beta(k+1)$ and $i_z(k+1)$ are transformed to $i_d(k+1)$, $i_q(k+1)$ and $i_{z1}(k+1)$ by Park transformation with Equation (31);

3) 15 groups of $i_d(k+1)$, $i_q(k+1)$, $i_{z1}(k+1)$ and $\omega(k+1)$ are substituted into Equation (28) to calculate the corresponding 15 values of the cost function F_c;

4) All F_c are ranked and compared, and the optimal voltage vector is selected with the minimal F_c from all basic voltage vectors. The optimal voltage vector is used to switch the inverter at $k+1$ time;

5) When $k > 0$, the state variables of system $i_\alpha(k)$, $i_\beta(k)$, $i_z(k)$, $\omega(k)$, $\theta(k)$ are measured by the current and speed sensors. Then, return to the step 2) for next control period.

5. **Simulation Result.** In Matlab/Simulink platform, the SPC system and PCC system with single-phase open fault in FPMSM are built as shown in Figure 5 and Figure 6. Compared with Figure 5 and Figure 6, SPC system needs to add the speed predictive model Equation (27) instead of adding PI controller to calculate the control variable i_q^*. In Figure 6, the cost function of the PCC strategy only consists of current error terms in Equation (33)

$$F_c' = \left(i_q^*(k+1) - i_q(k+1)\right)^2 + \left(i_d^*(k+1) - i_d(k+1)\right)^2 + \left(i_z^*(k+1) - i_z(k+1)\right)^2 \quad (33)$$

The parameters of the FPMSM are: DC-link voltage is: 120 V; rated power is: 5.5 kW; rated speed is: 550 r/min; pole pairs is: $p = 4$; stator resistance is: $R = 0.11\ \Omega$; inductance are: $L_\alpha = 0.001985$ H, $L_\beta = 0.00317$ H, $L_l = 0.0008$ H; flux linkage is: $\psi_f =$

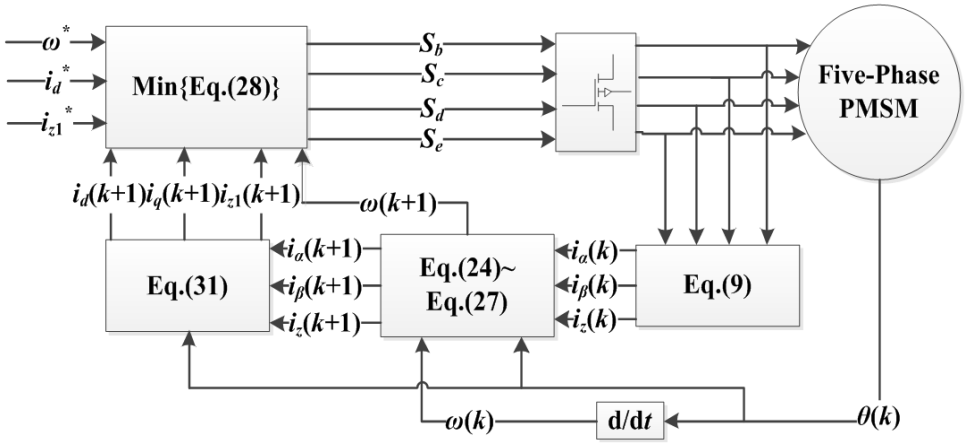

FIGURE 5. The structure of SPC strategy

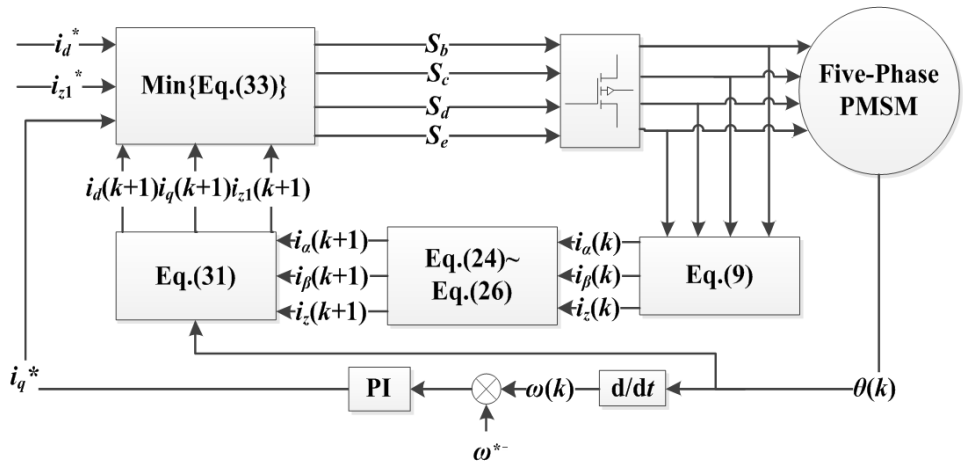

FIGURE 6. The structure of PCC strategy

0.05 Wb; motor inertia is: $J = 0.002$ kg·m^2; friction coefficient is: $B = 0.0001$ Nm·s/rad. The sampling period is: $T = 40$ μs; the weighting of the cost function in the SPC strategy are: $\lambda_\omega = 1000$, $\lambda_{id} = 1$, $\lambda_{iz} = 0.1$; the upper limits of output are: $i_{q\max} = 20$, $i_{d\max} = 0.5$, $i_{z\max} = 2.5$. In the PCC strategy, the output range of the PI controller is $[-20, 20]$; the proportional integral gain is: $k_p = 4$, $k_i = 30$. These control system parameters are optimal through the parameter tuning by the cross validation in simulations.

In simulation, the expected speed is $\omega^* = 12\pi$ rad/s when $0 \le t \le 0.15$ s and $\omega^* = 18\pi$ rad/s when $0.15 \le t \le 0.3$ s. The motor starts with a load torque with $T_L = 4$ N·m, and the load torque sharply adds to $T_L = 7$ N·m at $t = 0.1$ s.

In Figure 7, the speed response of SPC strategy has a steady-state speed error of ± 0.0015 rad/s. When the load increases sharply from 4 N·m to 7 N·m, the speed decreases by only 0.05 rad/s and reaches steady state within 0.0004 s. In Figure 8, the PCC strategy has a steady-state error of ± 0.075 rad/s. When the load increases, the speed decreases by 1.5 rad/s. Those results show that SPC strategy has a strong anti-interference ability, a smaller steady state error, and a faster dynamic response, by comparing with PCC strategy.

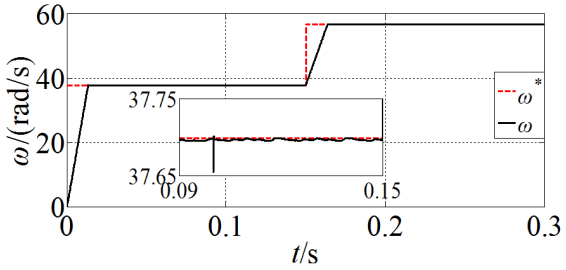

FIGURE 7. Speed of SPC

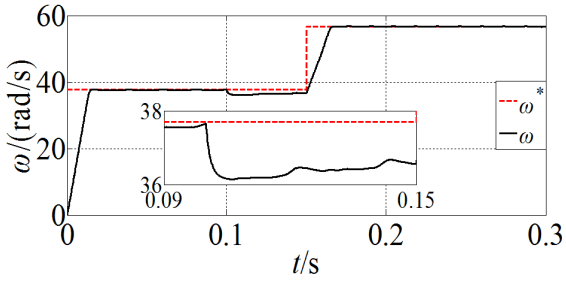

FIGURE 8. Speed of PCC

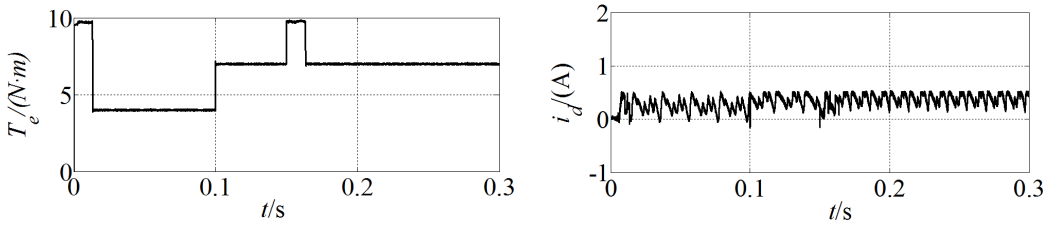

(a) (b)

FIGURE 9. Torque and d-axis current of SPC

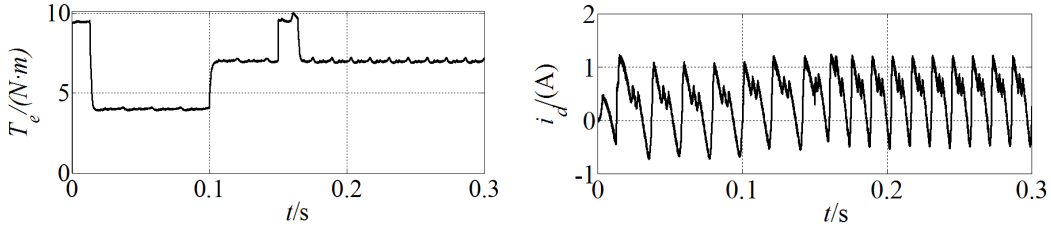

(a) (b)

FIGURE 10. Torque and d-axis current of PCC

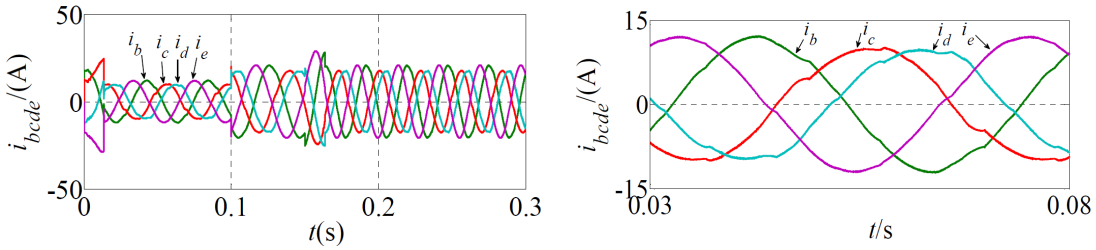

(a) (b)

FIGURE 11. Phase currents of SPC

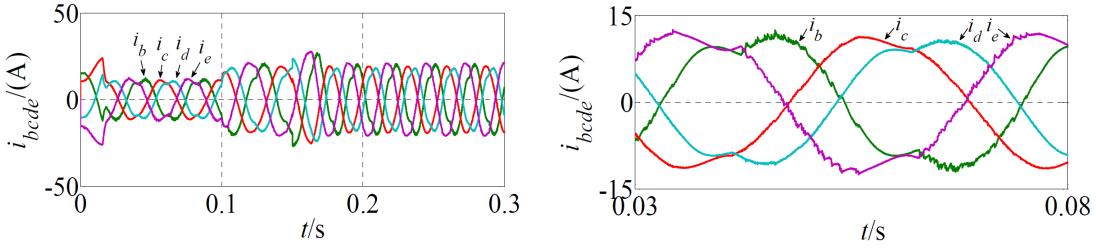

(a) (b)

FIGURE 12. Phase currents of PCC

Figure 9(a) shows the torque response by the SPC strategy. T_e increases rapidly to the maximum value during the dynamic process, to obtain the maximal acceleration of the motor. The steady-state torque fluctuation is about ±0.04 N·m. The maximal value of the d-axis current i_d in Figure 9(b) does not exceed 0.5 A, which satisfies the limited condition in the overcurrent protection term in Equation (29). Moreover, the steady-state fluctuations of the torque and d-axis current are consistent after the sudden load. However, Figure 10(a) shows the torque responses. The steady-state fluctuations of T_e approximately reach ±0.1 N·m and ±0.15 N·m with different loads, which is three times as SPC strategy. Figure 10(b) shows the d-axis current response i_d fluctuates from −0.6 to 1.2 A, which is twice as SPC strategy.

From Figure 11 and Figure 13, the response waveform of four-phase B, C, D, E current and α-β axis current of SPC strategy have a regular sinusoidal shape in single-phase open fault. From the detail of the phase current in Figure 11(b), the maximal amplitudes of the B-phase and E-phase currents are about 12 A, and the maximal amplitudes of the C-phase and D-phase currents are about 10 A, the ratio 12/10 = 1.2 is very close to 1.468/1.263 in Equation (22). The maximal amplitudes of B, C, D, E phase currents appear at about 0.0432 s, 0.0565 s, 0.0625 s and 0.0755 s, respectively. The current period

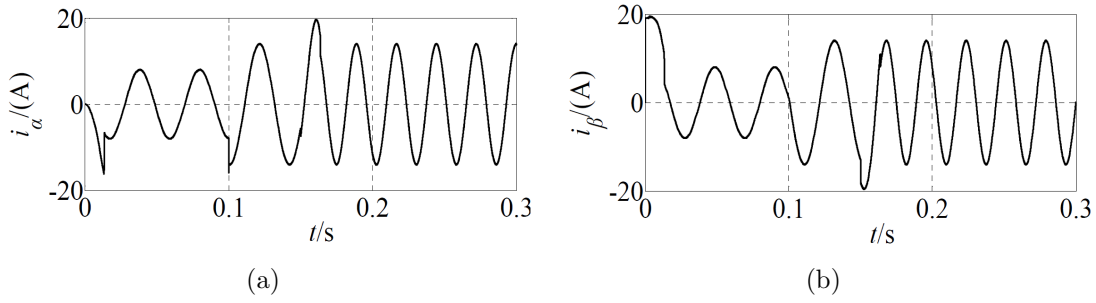

FIGURE 13. α-β axis currents of SPC

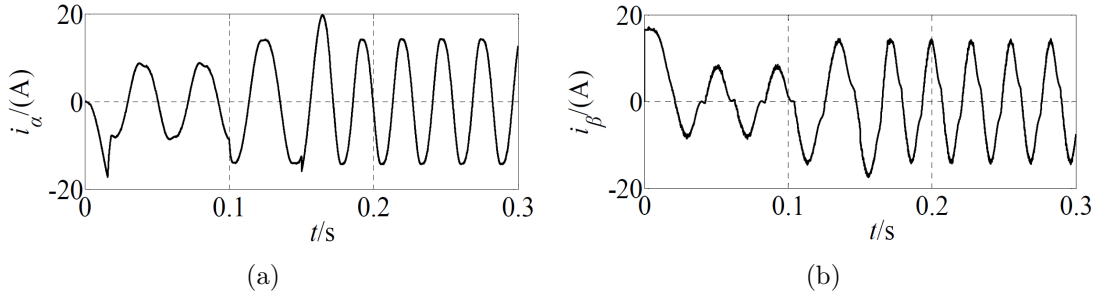

FIGURE 14. α-β axis currents of PCC

is about 0.0147 s, the phase differences between i_b and i_c, i_c and i_d, i_d and i_e are calculated as 114.8°, 51.8°, and 112.2°, respectively, which are close to those calculated by Equation (22). Equation (22) calculates the phase difference between i_b and i_c, i_c and i_d, i_d and i_e of $62.3° - (-49.6°) = 111.9°$, $117.7° - 62.3° = 55.4°$, $229.6° - 117.7° = 111.9°$. Therefore, the magnitudes and phases of B, C, D, E phase currents satisfy the relationship described in Equation (22), which is consistent with the constraint of minimal stator copper loss. From Figure 12 and Figure 14, the response waveforms of the phase currents and the α-β axis currents by PCC strategy are distorted which results in larger current fluctuations than the SPC strategy. PCC system is sensitive to the speed coupling term, and is difficult to obtain a satisfactory current control performance.

Therefore, for FPMSM in single-phase open fault, the SPC strategy can keep the motor running smoothly to obtain a superior system performance compared with PCC strategy.

6. **Conclusions.** In FPMSM with single-phase open fault, the PCC strategy cannot eliminate the coupling term between speed loop and current loop since α-β axis current is affected by the speed coupling term $\omega\psi_f \sin\theta/(2L_\alpha)$ and $\omega\psi_f \cos\theta/(2L_\beta)$ in the mathematical model. The fluctuations of speed and torque are obvious in PCC system. To overcome the shortcomings of PCC strategy, SPC strategy combining speed loop and current loop is proposed to suppress the coupling terms to regulate the speed in FPMSM. The speed error term is added to the cost function to regulate the speed directly, and the weight coefficient is introduced to balance the difference dimensions between the speed and the current. Moreover, the expected fault-tolerant current expression in single-phase open fault is calculated with the minimal stator copper loss. The simulation results show that SPC strategy can keep the motor running smoothly in FPMSM with single-phase open fault. Compared with PCC strategy, the steady-state errors of speed and torque are reduced to 1/50 and 1/3 respectively. SPC strategy has a superior system performance.

Acknowledgment. This work is partially supported by Natural Science Foundation of Fujian Province (2017J05101) and (2019H0007).

REFERENCES

[1] Z. Liu, Y. Li and Z. Zheng, A review of drive techniques for multiphase machines, *CES Trans. Electrical Machines and Systems*, vol.2, no.2, pp.243-251, 2018.

[2] L. D. Lillo, L. Empringham, P. W. Wheeler, S. Khwan-On, C. Gerada, M. N. Othman and X. Y. Huang, Multiphase power converter drive for fault-tolerant machine development in aerospace applications, *IEEE Trans. Ind. Electron.*, vol.57, no.2, pp.575-583, 2010.

[3] J. S. Thongam, M. Tarbouchi, A. F. Okou, D. Bouchard and R. Beguenane, Trends in naval ship propulsion drive motor technology, *IEEE Electrical Power & Energy Conference (EPEC)*, Halifax, pp.1-5, 2013.

[4] Z. Wang, X. Q. Wang, M. Cheng and Y. H. Hu, Comprehensive investigation on remedial operation of switch faults for dual three-phase PMSM drives fed by T-3L inverters, *IEEE Trans. Ind. Electron.*, vol.65, no.6, pp.4574-4587, 2018.

[5] M. Trabelsi, E. Semail, N. K. Nguyen and F. Meinguet, Open-switch and open-phase real time FDI process for multiphase PM synchronous motors, *IEEE the 25th International Symposium on Industrial Electronics (ISIE)*, Santa Clara, pp.179-185, 2016.

[6] H. Chang, S. Wang and P. Sun, Semi-active redundant fault tolerant control for an omnidirectional rehabilitative training robot with center of gravity shift, *ICIC Express Letters*, vol.13, no.2, pp.141-150, 2019.

[7] E. Levi, S. N. Vukosavic and M. Jones, Vector control schemes for series-connected six-phase two-motor drive systems, *IEE Proceedings – Electric Power Applications*, vol.152, no.2, pp.226-238, 2005.

[8] M. Bermudez, I. Gonzalez-Priet, F. Barrero, H. Guzman, X. Kestelyn and M. J. Duran, An experimental assessment of open-phase fault-tolerant virtual vector based direct torque control in five-phase induction motor drives, *IEEE Trans. Power Electron.*, vol.33, no.3, pp.2774-2784, 2018.

[9] C. S. Lim, E. Levi, M. Jones, N. A. Rahim and W. P. Hew, FCS-MPC-based current control of a five-phase induction motor and its comparison with PI-PWM control, *IEEE Trans. Ind. Electron.*, vol.61, no.1, pp.149-163, 2014.

[10] F. X. Wang, S. H. Li, X. Z. Mei, W. Xie, J. Rodríguez and R. M. Kennel, Model-based predictive direct control strategies for electrical drives: An experimental evaluation of PTC and PCC methods, *IEEE Trans. Ind. Inform.*, vol.11, no.3, pp.671-681, 2015.

[11] C. Xue, W. H. Song and X. Y. Feng, Finite control-set model predictive current control of five-phase permanent-magnet synchronous machine based on virtual voltage vectors, *IET Electr. Power Appl.*, vol.11, no.5, pp.836-846, 2017.

[12] J. Rodríguez, R. M. Kennel, J. R. Espinoza, M. Trincado, C. A. Silva and C. A. Rojas, High-performance control strategies for electrical drives: An experimental assessment, *IEEE Trans. Ind. Electron.*, vol.59, no.2, pp.812-820, 2012.

[13] Y. X. Luo and C. H. Liu, Pre- and post-fault tolerant operation of a six-phase PMSM motor using FCS-MPC without controller reconfiguration, *IEEE Trans. Veh. Technol.*, vol.68, no.1, pp.254-263, 2019.

[14] F. Barrero, J. Prieto, E. Levi, R. Gregor, S. Toral, M. J. Durán and M. Jones, An enhanced predictive current control method for asymmetrical six-phase motor drives, *IEEE Trans. Ind. Electron.*, vol.58, no.8, pp.3242-3252, 2011.

[15] H. Guzman, M. J. Duran, F. Barrero, B. Bogado and S. Toral, Speed control of five-phase induction motors with integrated open-phase fault operation using model-based predictive current control techniques, *IEEE Trans. Ind. Electron.*, vol.61, no.9, pp.4474-4484, 2014.

[16] M. Preindl and S. Bolognani, Model predictive direct speed control with finite control set of PMSM drive systems, *IEEE Trans. Power Electron.*, vol.28, no.2, pp.1007-1015, 2013.

[17] E. J. Fuentes, C. Silva, D. E. Quevedo and E. I. Silva, Predictive speed control of a synchronous permanent magnet motor, *IEEE International Conference on Industrial Technology*, Churchill, Australia, pp.1-6, 2009.

[18] A. Keshtkar, T. Maleki and A. Kalantarnia, Determination of optimum rails dimensions in Railgun by Lagrange's equations, *IEEE Trans. Magn.*, vol.45, no.1, pp.594-597, 2009.